REPORT DOCUMENTATION PAGE

Form Approved OMB NO. 0704-0188

1. AGENCY USE ONLY (Leave Blank)	2. REPORT DATE:	3. REPORT TYPE AND DATES COVERED Final Report 1-Sep-2002 - 30-Jun-2006

4. TITLE AND SUBTITLE
Low-Profile Radiators in Non-Periodic Wideband Arrays

5. FUNDING NUMBERS
DAAD190210398

6. AUTHORS
Jennifer T. Bernhard

8. PERFORMING ORGANIZATION REPORT NUMBER

7. PERFORMING ORGANIZATION NAMES AND ADDRESSES
University of Illinois - Urbana - Champaign
109 Coble Hall
801 S. Wright Street
Champaign, IL 61820 -6242

9. SPONSORING/MONITORING AGENCY NAME(S) AND ADDRESS(ES)
U.S. Army Research Office
P.O. Box 12211
Research Triangle Park, NC 27709-2211

10. SPONSORING / MONITORING AGENCY REPORT NUMBER
44493-EL.2

11. SUPPLEMENTARY NOTES
The views, opinions and/or findings contained in this report are those of the author(s) and should not contrued as an official Department of the Army position, policy or decision, unless so designated by other documentation.

12. DISTRIBUTION AVAILIBILITY STATEMENT
Approved for Public Release; Distribution Unlimited

12b. DISTRIBUTION CODE

13. ABSTRACT (Maximum 200 words)
The abstract is below since many authors do not follow the 200 word limit

14. SUBJECT TERMS
random phased array, wideband phased array, wideband antennas

15. NUMBER OF PAGES
Unknown due to possible attachments

16. PRICE CODE

17. SECURITY CLASSIFICATION OF REPORT	18. SECURITY CLASSIFICATION ON THIS PAGE	19. SECURITY CLASSIFICATION OF ABSTRACT	20. LIMITATION OF ABSTRACT
UNCLASSIFIED	UNCLASSIFIED	UNCLASSIFIED	UL

Report Title

Final Report for DAAD 19-02-1-0398: Low-Profile Radiators in Aperiodic Wideband Arrays

ABSTRACT

This report details our research progress during the course of this grant. This report includes development of new wideband antenna elements, strategies for cost-effective random arrays using these elements, and supporting computational codes. First, a summary of the development and analysis of the new antenna element developed under this project is provided. Measured and simulated results show that this new element can provide a 3:1 bandwidth (using VSWR = 3 as the bandwidth criteria typically used for wideband elements) with no degradation in radiation characteristics. Next, the results of our work on arrays of random subarrays are presented. Theoretical analyses show that rotating subarrays composed of random arrays can deliver performance close to that of a purely random array while making the array more cost effective and price competitive with alternatives that work over much smaller bandwidths. Parallel work on computational tools that enable wideband simulation of elements in random arrays is also discussed. Conclusions about this research and possible directions for future research are provided along with a listing of the publications sponsored by this project to date.

List of papers submitted or published that acknowledge ARO support during this reporting period. List the papers, including journal references, in the following categories:

(a) Papers published in peer-reviewed journals (N/A for none)

K. C. Kerby and J. T. Bernhard, "Sidelobe level and wideband behavior of arrays of random subarrays," IEEE Transactions on Antennas and Propagation, vol. 54, no. 8, pp. 2253-2262, Aug. 2006.

Number of Papers published in peer-reviewed journals: 1.00

(b) Papers published in non-peer-reviewed journals or in conference proceedings (N/A for none)

Number of Papers published in non peer-reviewed journals: 0.00

(c) Presentations

1. J. T. Bernhard, "Antennas for multifunction RF systems: current work and future directions," Poster presentation, Proc. DARPA/ONR Workshop on Future Directions for Multifunction RF Systems, November 2003.

Number of Presentations: 1.00

Non Peer-Reviewed Conference Proceeding publications (other than abstracts):

Number of Non Peer-Reviewed Conference Proceeding publications (other than abstracts): 0

Peer-Reviewed Conference Proceeding publications (other than abstracts):

1. K. C. Kerby and J. T. Bernhard, “Arrays of random subarrays for wideband applications,” in Proc. GOMACTech-2006, San Diego, CA, March 2006.
2. (Invited paper) J. T. Bernhard, K. C. Kerby, G. Cung, and P. E. Mayes, “Wideband random phased arrays: theory and design,” in Proc. IEE Seminar on Wideband and Multi-band Antennas and Arrays, Sept. 2005.
3. J. T. Bernhard, G. Cung, K. C. Kerby, and P. E. Mayes, “Development of Wideband Random Phased Arrays Composed of Modified Canted Sector Antennas,” in Proc. 2005 IEEE/ACES International Conference on Wireless Communications and Applied Computational Electromagnetics, 3-7 April 2005, pp. 229-232.
4. J. T. Bernhard, G. Cung, K. C. Kerby, and P. E. Mayes, “Wideband Random Phased Arrays: Cost-effective Multifunction Performance,” in Proc. GOMACTech-2005, Las Vegas, NV, March 2005.
5. K. C. Kerby and J. T. Bernhard, “Array of rotated random subarrays,” in Proc. 2004 Antenna Applications Symposium, Sept. 2004, pp. 293-307.
6. K. C. Kerby and J. T. Bernhard, “Wideband periodic array of random subarrays,” Proc. 2004 IEEE/URSI Int. Symp. on Antennas and Propagation, Monterey, CA, v. 1, June 2004, pp. 555-558.
7. G. Cung, J. Fladie, P. E. Mayes, and J. T. Bernhard, “Investigation of canted compound sector antennas for wideband periodic arrays,” Proc. 2004 IEEE/URSI Int. Symp. on Antennas and Propagation, Monterey, CA, v. 2, June 2004, pp. 1887-1890.
8. G. Cung, J. Fladie, P. E. Mayes, and J. T. Bernhard, “Wideband low-profile canted antennas for broadside radiation in aperiodic arrays,” Proc. GOMACTech-2004, Monterey, CA, March 2004, p.167-170.
9. J. T. Bernhard, “Linking electromagnetic design to system performance: measuring bit error rate as a function of antenna properties and more,” in Proc. URSI National Radio Science Meeting, Jan. 2004, p. 78.
10. J. T. Bernhard, B. Herting, P. Mayes, N. Chen, and E. Michielssen, “Wideband low-profile canted antennas for array applications,” in Proc. 2003 IEEE/URSI Int. Symp. on Antennas and Propagation, URSI, June 2003, p. 694.
11. J. T. Bernhard, B. Herting, N.-W. Chen, P. Mayes, and E. Michielssen, “Low Profile Radiators for Wideband Arrays,” Proc. GOMACTech-2003, Tampa, FL, April 2003.

Number of Peer-Reviewed Conference Proceeding publications (other than abstracts): 11

(d) Manuscripts

1. G. Cung and J. T. Bernhard, “Preliminary radiation model for a wideband triangular canted sector antenna,” Manuscript in preparation for submission to IEEE Antennas and Wireless Propagation Letters.

Number of Manuscripts: 1.00

Number of Inventions:

Graduate Students

NAME	PERCENT_SUPPORTED	
Kiersten K. Kerby	0.50	No
Garvin Cung	0.50	No
FTE Equivalent:	**1.00**	
Total Number:	**2**	

Names of Post Doctorates

NAME	PERCENT_SUPPORTED
FTE Equivalent:	
Total Number:	

Names of Faculty Supported

NAME	PERCENT_SUPPORTED	National Academy Member
Jennifer T. Bernhard	0.08	No
Eric Michielssen	0.04	No
Paul Mayes	0.04	No
FTE Equivalent:	**0.16**	
Total Number:	**3**	

Names of Under Graduate students supported

NAME	PERCENT_SUPPORTED	
Joshua Fladie	0.10	No
Morgan Reeder	0.10	No
FTE Equivalent:	**0.20**	
Total Number:	**2**	

Names of Personnel receiving masters degrees

NAME	
Kiersten C. Kerby	No
Garvin Cung	No
Total Number:	**2**

Names of personnel receiving PHDs

NAME
Total Number:

Names of other research staff

NAME	PERCENT_SUPPORTED
FTE Equivalent:	
Total Number:	

Sub Contractors (DD882)

Inventions (DD882)

Final Report for DAAD 19-02-1-0398
Dates: 9/1/2002-6/30/2006
Title: Low-Profile Radiators in Aperiodic Wideband Arrays

PI: Prof. Jennifer T. Bernhard
CO-PIs: Prof. Paul E. Mayes and Prof. Eric Michielssen
Electromagnetics Laboratory
Department of Electrical and Computer Engineering
University of Illinois at Urbana-Champaign

Submitted November 22, 2006

Table of Contents

Abstract

This report details our research progress during the course of this grant. This report includes development of new wideband antenna elements, strategies for cost-effective random arrays using these elements, and supporting computational codes. First, a summary of the development and analysis of the new antenna element developed under this project is provided. Measured and simulated results show that this new element can provide a 3:1 bandwidth (using VSWR = 3 as the bandwidth criteria typically used for wideband elements) with no degradation in radiation characteristics. Next, the results of our work on arrays of random subarrays are presented. Theoretical analyses show that rotating subarrays composed of random arrays can deliver performance close to that of a purely random array while making the array more cost effective and price competitive with alternatives that work over much smaller bandwidths. Parallel work on computational tools that enable wideband simulation of elements in random arrays is also discussed. Conclusions about this research and possible directions for future research are provided along with a listing of the publications sponsored by this project to date.

1. Introduction

Wideband antennas may be used to decrease the number of antennas needed on platforms that require operation over a large frequency band. Some typical examples of wideband antennas include TEM horns [1, 2, 3] and Vivaldi [4, 5, 6] tapered slot antennas. Although both types do offer wideband operation, they are often not suitable for certain situations due to their large thickness, weight, and complicated feed networks. In order to resolve these issues, a thin low-profile antenna is needed. The attractive features of canted sector antennas, which are triangular, conducting sectors with various geometries canted above ground planes, are simplicity and wide impedance bandwidth. Band limits are established by variations in the radiation pattern. These antennas are intended for implementation in wideband aperiodic arrays for high-speed communications.

This report details our research progress during the course of this grant. This work includes development of new wideband antenna elements, strategies for cost-effective random arrays using these elements, and supporting computational codes. Section 2 provides a summary of the development and analysis of the new antenna element developed under this project. Section 3 summarizes the results of our work on arrays of random subarrays that promise to make this architecture cost effective and price competitive with less functional alternatives. Parallel work on computational tools that enable wideband simulation of elements in random arrays is discussed in Section 4. Our conclusions about this research and possible directions for future research are provided in Section 5 along with a listing of the publications sponsored by this project to date.

2. Wideband Low Profile Antenna Element

The project began with examination of simple canted sector antennas [7, 8]. The attractive features of canted sector antennas, which are triangular, conducting sectors with various geometries canted above ground planes, are simplicity and wide impedance bandwidth. Band limits are established by variations in the radiation pattern. With the simple sector, the radiation pattern exhibits some depressions close to broadside that are unacceptable for adequate scanning of the array. To improve the broadside operation of the element, several changes were implemented. We have developed a new design that combines a number of geometrical changes, including a taper in the main triangular region and upward bends in the corners. This structure is shown in Figure 1 along with measured and simulated impedance data. From 2 – 6 GHz, the element has a VSWR that is always less than about 2.5:1.

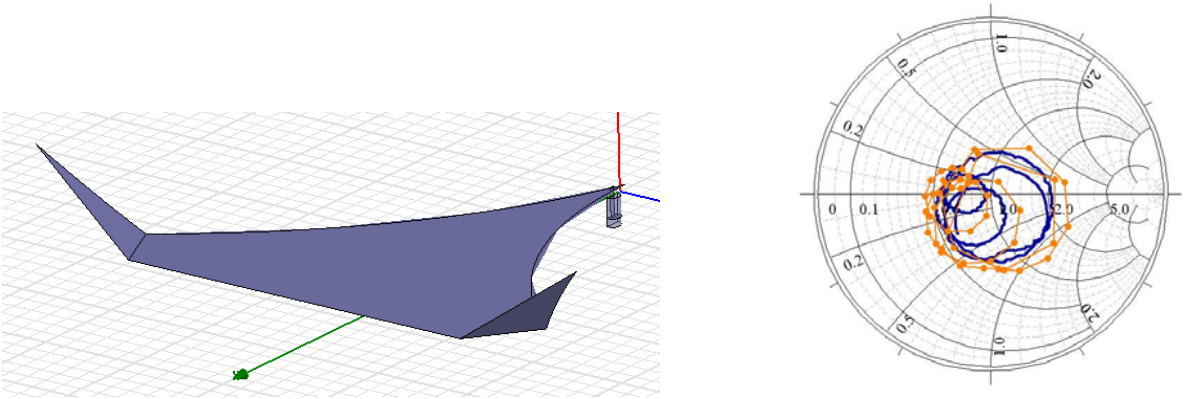

Figure 1: Modified canted sector antenna (left) with measured (blue-solid) and simulated (orange-dotted) impedance from 2-6 GHz.

Figure 2 shows the dimensions of the tapered sector with bent corners. The piece-wise taper along the side edges of the sector antenna is defined by three angles; this taper resembles a quadratic function. The corners were bent upwards by an angle ζ with respect to the plane of the sector, and a cant angle of $\alpha = 5^{\circ}$ was used. The same ground plane and excitation method used for the simple sector was applied.

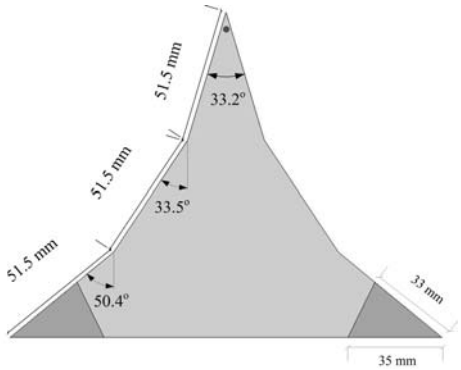

Figure. 2: Geometry of the tapered sector with bent corners.

The antenna was first simulated with corner bends of $\zeta = 0^{\circ}$ (no bend), 20°, and 40°. As expected, the input impedance improved with increasing ζ. The case with $\zeta = 20^{\circ}$ had the best match of the simulated cases. The simulated radiation patterns showed the removal of the depressions at 3.6 and 4.4 GHz with $\zeta \geq 20^{\circ}$. However, the corner bends were not able to remove the null at 2 GHz. Even so, there is good broadside behavior from 2.2 GHz to at least 6 GHz; simulations above 6 GHz were not performed. As expected, the antenna continues to exhibit good impedance characteristics as the frequency increases. A corner bend angle of $\zeta = 20^{\circ}$ was sufficient in the simulations to satisfy the broadside pattern conditions, and maintain the low-profile property (this antenna has a vertical dimension of 22.3 mm and the simple sector with $\alpha = 10^{\circ}$, $\beta = 67^{\circ}$ and $L = 125$ mm in [9] has a vertical dimension of 22.1 mm), and was thus fabricated and is shown in Figure 3. The element taper reduces the VSWR at the lower end of the band compared to that of the simple sector.

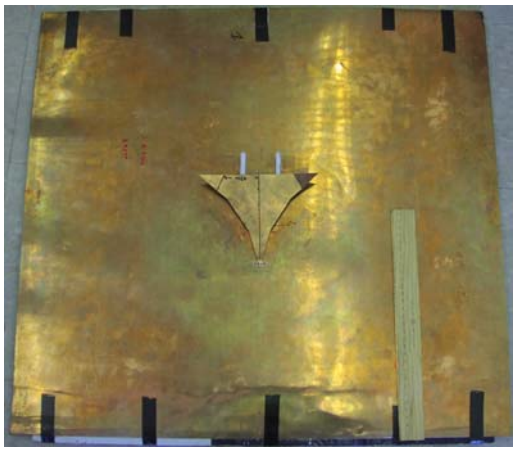

Figure 3: Fabricated tapered sector with bent corners.

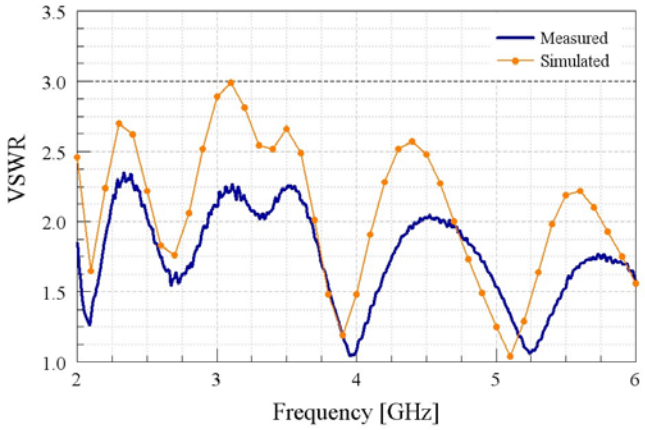

Figure 4: VSWR of the tapered sector with bent corners.

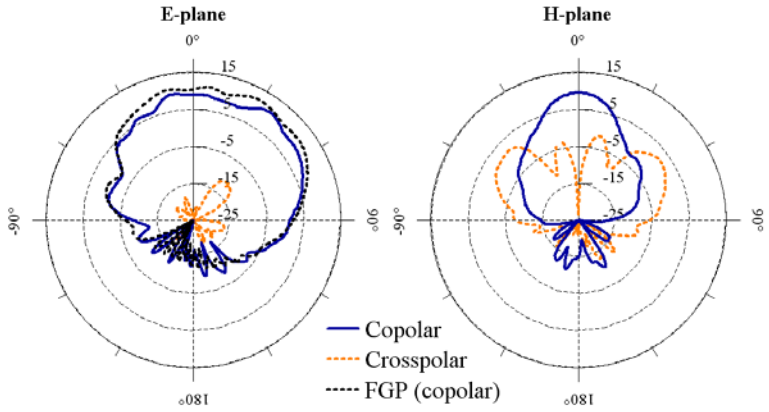

Figure 5: Measured and simulated (FGP) radiation patterns at 3.2 GHz of the tapered sector with bent corners.

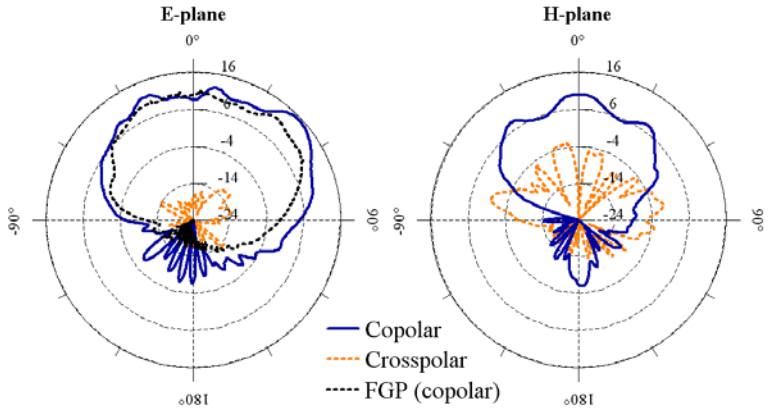

Figure 6: Measured and simulated (FGP) radiation patterns at 4.4 GHz of the tapered sector with bent corners.

Figure 4 presents the measured and simulated VSWR. There was a slight over-estimation in the simulated results compared to the measured results, but the overall input impedance trends agree well with each other. Figures 5 and 6 show the measured and simulated (E-plane copolar only) patterns at 3.2 GHz and 4.4 GHz, respectively, with the FGP designation indicating simulated results obtained with the TD-AIM simulator developed in this project. The depressions that were present in the simple sector were indeed alleviated and a continuous broadside pattern bandwidth with a 2.5:1 VSWR from 2.2–6 GHz was achieved.

The antenna has been analyzed extensively. We are presently finishing an analytical model of both the simple sector as well as this most promising permutation to support new designs and scaling in the future. Two journal papers on this element are in preparation. In the course of this research, Mr. Garvin Cung, the graduate student who developed this antenna element, completed his M.S. thesis on this topic [10] and graduated from the University of Illinois at Urbana-Champaign in August 2005. He is presently employed with Northrop Grumman in Baltimore, Maryland.

3. Random Array Studies

While truly random arrays may prove too costly to fabricate efficiently using today's methods, we are developing design approaches that provide good sidelobe performance over frequency while remaining practical and cost-effective to fabricate and operate. Our approach is to use a smaller random array as a subarray building block. A brief discussion of the results of three different variations is provided here.

We have studied periodic arrays of random subarrays (PARS) that consist of small rectangular random subarrays arranged periodically [11]. Such a configuration is shown in Figure 7(a). For an array of a given aperture size and number of elements, the robust wideband performance of a random array is preserved in a geometrically simpler design, but with somewhat higher sidelobes than a purely random array of the same size. As a result, from a performance standpoint a purely random array is more effective, and the reason to use a PARS would be that one wanted to use a certain number of elements to achieve some desired gain in a geometrically simpler package than the purely random array.

Another approach is to rotate the subarrays relative to one another in the array, creating arrays of periodically rotated random subarrays (ARRS-P), depicted in Figure 7(b) [12, 13]. Our work shows that if the number of elements in the subarrays is larger than a threshold value for a particular frequency range, both the PARS and ARRS have very stable array factors and can easily be designed so that their sidelobe levels remain below a specified value over the entire operating band. However, the ARRS has a lower threshold value, as shown in Figure 8, resulting in lower element density and consequently an extended lower frequency limit. The number of elements required to achieve a specified sidelobe level is reduced, which results in arrays with fewer elements and feed lines for the same sidelobe level or in lower sidelobe levels for the same number of elements. Using fewer elements will result in lower aperture gain, but may also result in a cost savings over multiple traditional periodic arrays that perform comparable functions.

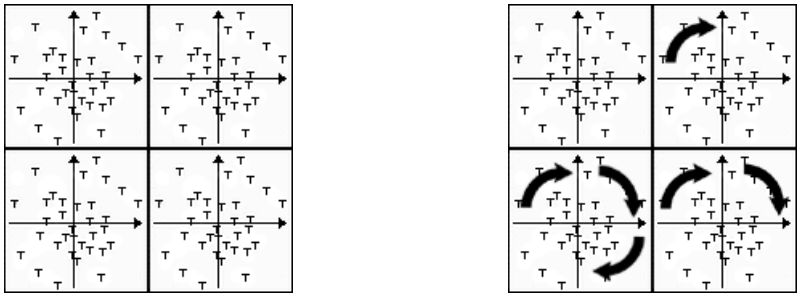

(a) (b)

Figure 7: (a) Periodic array of random subarray (PARS). (b) Array of rotated random subarrays (ARRS).

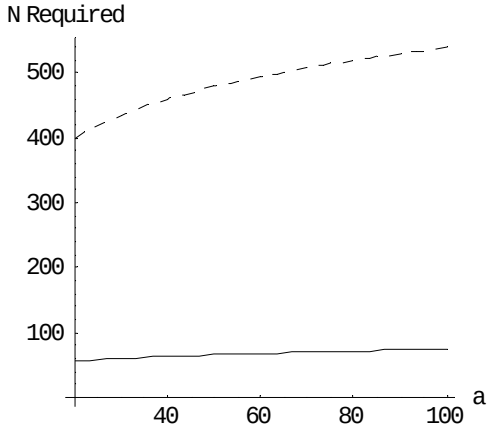

Figure 8: Number of elements required to achieve a –20 dB sidelobe level with 85% probability vs. *a* (subarray side length in wavelengths), which depends linearly on frequency, for PARS (dashed line) and an ARRS-P (solid line) with four subarrays each [12].

Finally, the concept of subarray rotation is generalized to allow random rotations. In an array of randomly rotated random subarrays (ARRS-R), the pattern of rotations is not deterministic. For simplicity, we require that the subarrays not overlap. As with the PARS and ARRS-P, the likely

behavior of the arrays can be predicted using probabilistic methods. Results indicate that the ARRS-R can achieve lower sidelobe levels with fewer elements per subarray as more subarrays are added [14, 15]. This is in contrast to the PARS and the ARRS-P, in which addition of more subarrays eventually ceases to improve the sidelobe level performance of the complete array.

A journal paper on this random array study has been published [14] and is attached to this report as Appendix 1. In the course of this research, Ms. Kiersten Kerby completed her M.S. thesis on this topic [15] and earned the M.S. degree from the University of Illinois at Urbana-Champaign in May 2005. She spent the summer of 2005 in an engineering internship at Ball Aerospace in Colorado, and she is now continuing for her Ph.D. at the University of Illinois under the direction of Prof. Bernhard.

We requested a no-cost extension in order to complete a measurement demonstration of these random subarray concepts using optical techniques. The screen designs were generated using our established procedures, and slots are used as the radiating elements. Due to unforeseeable delays related to the breakdown of fabrication equipment, we were delayed in fabricating the first designs until May 2006. After fabrication, we determined that the conductive coating on the screens was not thick enough, allowing light to pass through. We are currently working on a slightly modified fabrication technique that will result in thicker conducting film deposition in the optical screens. Once the new screens are fabricated, we will measure the beam patterns produced using uniform laser illumination to assess the feasibility of several of our proposed approaches for arrangement of random subarrays in large arrays.

4. Computational Tool Development

A time domain integral equation solver that is being used to quickly and accurately simulate these antennas has been developed at the University of Illinois under this grant. Specifically, a marching-on-time (MOT) algorithm for solving a time-domain electric field integral equation pertinent to the analysis of free-standing antennas was constructed. Given a bandlimited excitation, the algorithm solves for induced surface currents on the conductors using a time domain method-of-moments formulation. For a geometry modeled using N_s surface unknowns, the computational complexity of this algorithm scales as $O(N_t N_s^2)$ for N_t time steps of simulation. Using a parallel FFT-based accelerator, the time-domain adaptive integral method (TD-AIM), the cost of solution is reduced to $O(N_t N_s \log^2 N_s)$ operations for the antennas shown below. The solver employs the message passing paradigm via the MPI standard for communication between processors and utilizes the Fastest Fourier transform in the West (FFTW) library to compute parallel FFTs. Thanks to the near-ideal parallel performance of the solver, we have been able to analyze the broadband characteristics of antennas that involve $N_s > 100,000$ degrees of freedom using supercomputers with tens of processors in practical amounts of time.

Various antenna shapes have been investigated using the TD-AIM based simulator to investigate their radiation patterns over a broad range of frequencies [16, 17]. The simulations shown in Section 2 with finite ground planes were performed with this simulator and agree well with measured results.

Further array simulations will rely mainly on array factor multiplications of element patterns due to the otherwise extremely large computational space required.

5. Conclusions and Directions for Future Work

Our work on the canted sector antenna led to modified designs with good impedance and radiation characteristics that can meet a number of different array scan requirements. We continue to work on analytical models for all of these designs to enable further refinement as well as scaling for new frequency bands of interest. In the future, more rigorous studies on the corner bend locations and different quadratic tapers will be pursued to improve the antenna performance further.

Our work in random arrays has shown very promising results. Work on the possible packaging and arrangement of random subarrays may continue, including investigation of the effects of small numbers of elements and the possibility of recursive rotation arrangements that may duplicate the behavior of truly random arrays.

Finally, we will continue to pursue the measurement demonstration using optical techniques during the last period of this project we will calculate complete radiation patterns for arrays with random subarrays composed of these wideband elements. During this process, we will also evaluate scan capabilities and investigate the possibility of using the wideband element's endfire characteristics at higher frequencies to extend scan angle ranges.

6. Publications and Presentations Sponsored by this Grant

1. G. Cung and J. T. Bernhard, "Preliminary radiation model for a wideband triangular canted sector antenna," Manuscript in preparation for submission to *IEEE Antennas and Wireless Propagation Letters*.
2. K. C. Kerby and J. T. Bernhard, "Sidelobe level and wideband behavior of arrays of random subarrays," *IEEE Transactions on Antennas and Propagation*, vol. 54, pp. 2253-2262, Aug. 2006.
3. (Invited Paper) J. T. Bernhard, K. Kerby, G. Cung, and P. E. Mayes, "Wideband random phased arrays: theory and design," *Proc. IEE Seminar on Wideband and Multi-band Antennas and Arrays*, University of Birmingham, 7 September 2005.
4. G. Cung, *Design and Analysis of Wideband Canted Sector Antennas for Use in Aperiodic Arrays*, M.S. Thesis, University of Illinois at Urbana-Champaign, August 2005.
5. K. C. Kerby, *Sidelobe Level and Wideband Behavior of Arrays of Random Subarrays*, M.S. Thesis, University of Illinois at Urbana-Champaign, May 2005.
6. J. T. Bernhard, G. Cung, K. C. Kerby, and P. E. Mayes, "Wideband random phased arrays: cost-effective multifunction performance," *Proc. GOMACTech-2005*, Las Vegas, NV, March 2005.
7. J. T. Bernhard, G. Cung, K. C. Kerby, and P. E. Mayes, "Development of wideband random phased arrays composed of modified canted sector antennas," *Proc. 2005 IEEE/ACES International Conference on Wireless Communications and Applied Computational Electromagnetics*, April 2005.
8. K. C. Kerby and J. T. Bernhard, "Array of rotated random subarrays," *Proc. 2004 Antenna Applications Symposium*, Sept. 2004, pp. 293-307.

9. K. C. Kerby and J. T. Bernhard, “Wideband periodic array of random subarrays,” *Proc. 2004 IEEE/URSI Int. Symp. on Antennas and Propagation*, Monterey, CA, v. 1, June 2004, pp. 555-558.
10. G. Cung, J. Fladie, P. E. Mayes, and J. T. Bernhard, “Investigation of canted compound sector antennas for wideband periodic arrays,” *Proc. 2004 IEEE/URSI Int. Symp. on Antennas and Propagation*, Monterey, CA, v. 2, June 2004, pp. 1887-1890.
11. G. Cung, J. Fladie, P. E. Mayes, and J. T. Bernhard, “Wideband low-profile canted antennas for broadside radiation in aperiodic arrays,” *Proc. GOMACTech-2004*, Monterey, CA, March 2004, p.167-170.
12. J. T. Bernhard, “Linking electromagnetic design to system performance: measuring bit error rate as a function of antenna properties and more,” in *Proc. URSI National Radio Science Meeting*, Jan. 2004, p. 78.
13. J. T. Bernhard, “Antennas for multifunction RF systems: current work and future directions,” Poster presentation, *Proc. DARPA/ONR Workshop on Future Directions for Multifunction RF Systems*, November 2003.
14. J. T. Bernhard, G. H. Huff, J. Feng, S. Zhang, and G. Cung, “Reconfigurable portable antenna systems for high-speed wireless communication,” *Proc. 2003 IEEE Topical Conf. on Wireless Communication Technology*, October 2003, pp. 82-83.
15. J. T. Bernhard, B. Herting, P. Mayes, N. Chen, and E. Michielssen, “Wideband low-profile canted antennas for array applications,” in *Proc. 2003 IEEE/URSI Int. Symp. on Antennas and Propagation*, URSI, June 2003, p. 694.
16. J. T. Bernhard, B. Herting, N.-W. Chen, P. Mayes, and E. Michielssen, “Low Profile Radiators for Wideband Arrays,” *Proc. GOMACTech-2003*, Tampa, FL, April 2003.

7. References

[1] E. L. Holzman, "A wide band TEM horn array radiator with a novel microstrip feed," *Proc. 2000 IEEE Int. Conf. on Phased Array Systems and Technology*, 441-444 (2000).

[2] L. Li-Chung, T. Chang, and W. D. Burnside, "An ultrawide-bandwidth tapered resistive TEM horn antenna," *IEEE Trans. On Antennas and Propagat.*, 48(12), 1848-1857 (Dec. 2000).

[3] D. T. McGrath, "Blindness effects in ground plane-backed TEM horn arrays," *Proc. 1998 AP-S IEEE Int. Symp. on Antennas and Propagation*, 2, 1024-1027 (1998).

[4] A. O. Boryssenko and D. H. Schaubert, "Single-polarized, dielectric-free, Vivaldi tapered slot phased array: performance prediction," *Proc. 2001 AP-S IEEE Int. Symp. on Antennas and Propagation*, 2, 436-439 (2001).

[5] D. H. Schaubert, "Wide-band phased arrays of Vivaldi notch antennas," *Proc. Tenth Int. Conf. on Antennas and Propagation*, 1, 6-12 (1997).

[6] N. Schuneman, J. Irion, and R. Hodges, "Decade bandwidth tapered notch antenna array element," *Proc. 2001 Antenna Applications Symposium*, Allerton Park, Monticello, Illinois, 280-294 (2001).

[7] J. T. Bernhard, B. Herting, N.-W. Chen, P. Mayes, and E. Michielssen, "Low profile radiators for wideband arrays," *Proc. GOMACTech-2003*, Tampa, FL, April 2003.

[8] J. T. Bernhard, B. Herting, J. Fladie, D. Chen, and P. E. Mayes, "Investigation of wideband low-profile canted antennas for broadside radiation in aperiodic arrays," *Proc. 2003 Antenna Applications Symposium*, Allerton Park, Monticello, Illinois, 318-326 (2003).

[9] G. Cung, J. Fladie, P. E. Mayes, and J. T. Bernhard, "Investigation of canted compound sector antennas for wideband aperiodic arrays," in *Proc. 2004 IEEE/URSI Int. Symp. on Antennas and Propagation*, Monterey, CA, vol. 2, June 2004, pp. 1887-1890.

[10] G. Cung, *Design and Analysis of Wideband Canted Sector Antennas for Use in Aperiodic Arrays*, M.S. Thesis, University of Illinois at Urbana-Champaign, August 2005.

[11] K. C. Kerby and J. T. Bernhard, "Wideband periodic array of random subarrays," *Proc. 2004 AP-S IEEE Int. Symp. on Antennas and Propagation*, vol. 1, 2004, pp. 555-558.

[12] K. C. Kerby and J. T. Bernhard, "Array of rotated random subarrays," *Proc. 2004 Antenna Applications Symposium*, Sept. 2004, pp. 293-307.

[13] P. S. Hall and M. S. Smith, "Sequentially rotated arrays with reduced sidelobe levels," *IEE Proc. Microwaves, Antennas and Propagat.*, vol. 141, no. 4, Aug. 1994, pp. 321-325.

[14] K. C. Kerby and J. T. Bernhard, "Sidelobe level and wideband behavior of arrays of random subarrays," In review at *IEEE Transactions on Antennas and Propagation.*

[15] K. C. Kerby, *Sidelobe Level and Wideband Behavior of Arrays of Random Subarrays*, M.S. Thesis, University of Illinois at Urbana-Champaign, May 2005.

[16] A. E. Yilmaz, J. M. Jin, and E. Michielssen, "Time domain adaptive integral method for surface integral equations," *IEEE Trans. Antennas and Propagat.*, vol. 52, pp. 2692–2708, Oct. 2004.

[17] A. E. Yilmaz, J. M. Jin, and E. Michielssen, “A parallel time-domain adaptive integral method based hybrid field-circuit simulator,” *Proc. IEEE Antennas Propagat. Soc. Int. Symp. Digest*, vol. 3, 2004, pp. 3309–3312.

Appendix 1

K. C. Kerby and J. T. Bernhard, “Sidelobe level and wideband behavior of arrays of random subarrays,” *IEEE Transactions on Antennas and Propagation*, vol. 54, pp. 2253-2262, Aug. 2006.

Sidelobe Level and Wideband Behavior of Arrays of Random Subarrays

Kiersten C. Kerby, *Student Member, IEEE*, and Jennifer T. Bernhard, *Senior Member, IEEE*

***Abstract*—We propose an extension to the concept of random antenna arrays. Three new array geometries are introduced which are intended to incorporate the wide bandwidth capability of a random array while having simplified geometry to increase their suitability for lower-cost applications. The behaviors of the periodic array of random subarrays, array of periodically rotated random subarrays, and array of randomly rotated random subarrays are each characterized probabilistically. Results indicate that subarray rotation can lower the sidelobe level of the array factor. An example of the design process is presented with calculated array factors.**

***Index Terms*—Antenna arrays, random arrays, subarrays, wideband arrays.**

I. Introduction

FOR many applications, it is common to use periodic antenna arrays because they are relatively simple to design and manufacture. However, as the importance of wide bandwidths and multifrequency operation has increased, it has become evident that there are significant disadvantages to the use of periodic arrays. For instance, because the element spacing of periodic arrays is proportional to the wavelength of operation, the patterns of periodic arrays change drastically and quickly develop grating lobes in response to changes in frequency. In the past, these have not been major issues because systems typically operated at only one frequency and with narrower bandwidths. But as the trend of increasing bandwidths and multifrequency systems continues, it will be important for array design to overcome those obstacles. Aperiodic element placement offers one possible solution.

When aperiodic arrays were first investigated in the 1960s, their utility was based largely in their capability for high resolution with relatively few elements, as well as wide scan angle capability. They were considered a lower-cost replacement for the large, mechanically scanned reflector antennas used in remote sensing. Initially, designers of aperiodic arrays often used preassigned element locations, in essentially arbitrary distributions [1]. Because of the limitations of computers at the time, optimization was somewhat impractical and attempts at it led to only locally optimum element placement [2], [3]. Lo [4] then proposed treating large antenna arrays probabilistically, even though the problem was not originally probabilistic. This approach—probabilistically analyzing arrays with random element placement—represented the formal introduction of random arrays and a systematic method of analyzing them. Investigation of random arrays produced a general understanding of their behavior and advantages [5] and found that, in fact, most deterministic aperiodic array design methods produced results that were not significantly better than random [6]. Arrays that were quasi-optimized using dynamic programming were the only ones whose performance was appreciably better than random element placements. Further work on the subject included some interesting special cases of the purely random array, such as binned [7] and nearest-neighbor constrained [8] random arrays.

Aperiodic arrays have very stable patterns over wide ranges of frequency, so they are well suited to operating over large bandwidths. However, the aperiodicity that yields this behavior also makes such arrays difficult to fabricate. It is far simpler to manufacture a repetitive structure such as a periodic array. Recently, work on aperiodic arrays has often been concerned with optimization of their patterns. Naturalistic optimization methods such as genetic [9] and particle-swarm [10] algorithms are certainly capable of producing arrays with performance better tailored to their particular applications. However, since the problem considered here is largely one of subarray arrangement, this work addresses random arrays. Once some effective geometric simplification methods are found, they may later be combined with optimization techniques. Since random arrays by definition choose one element distribution out of the entire set of all possible arrays, this approach can be applied to other types of aperiodic arrays.

The following sections detail attempts at geometry simplification, including a periodic array of random subarrays (PARS) and arrays of periodically and randomly rotated random subarrays (ARRS-P and ARRS-R, respectively). A comparison between the three types is presented, followed by remarks on the results of the investigation and possibilities for future work.

II. Three Geometries for an Array of Random Subarrays

The random element placement of purely random arrays makes them more difficult to manufacture than a periodic array. Three array geometries were developed in an attempt to mitigate this problem while preserving the wide bandwidth response and high failure tolerance of purely random arrays. This section presents the geometries of all three types.

The first type of array, a periodic array of random subarrays (PARS), is composed of many identical random subarrays arranged in a periodic grid (Fig. 1).

Manuscript received July 31, 2005; revised January 22, 2006. This work was supported by the Army Research Office under Grant DAAD19-02-1-0398.

The authors are with the Electromagnetics Laboratory, Department of Electrical and Computer Engineering, University of Illinois at Urbana-Champaign, Urbana, IL 61801 USA (e-mail: jbernhar@uiuc.edu).

Digital Object Identifier 10.1109/TAP.2006.879195

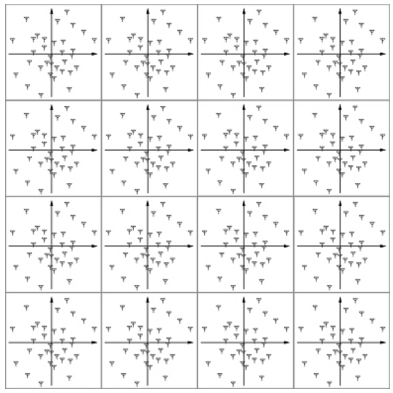

Fig. 1. Geometry of PARS.

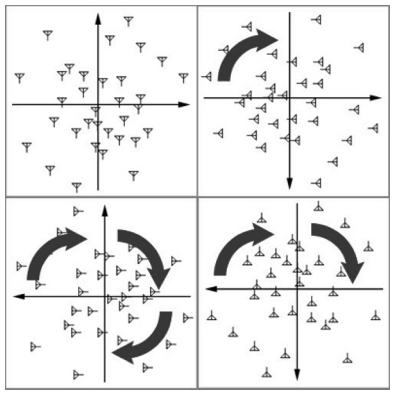

Fig. 2. ARRS-P geometry.

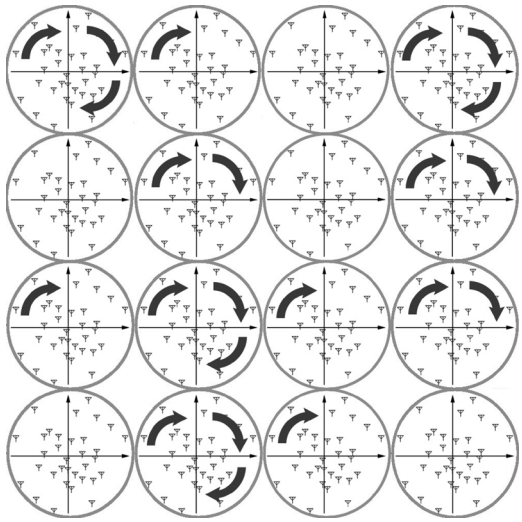

Fig. 3. Geometry of a particular ARRS-R array, with round subarrays and $M = 4$.

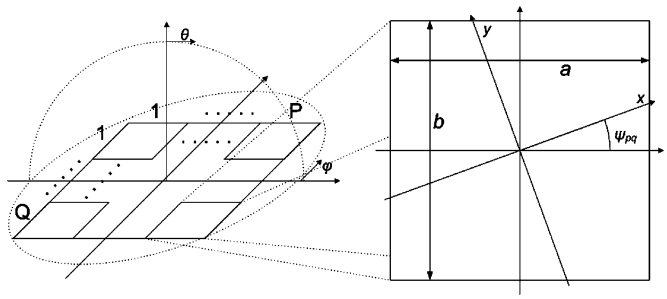

Fig. 4. Illustration of variable definitions. Left: subarray indices and global coordinate system. Right: subarray rotation, dimensions, and local coordinate system.

The next variation is an array of periodically rotated random subarrays (ARRS-P). The identical subarrays of the PARS are rotated in the azimuthal plane in a pattern that repeats over blocks of four subarrays. In each block, the coordinates of the subarrays' centers are $(-(a/2), a/2)$, $(a/2, a/2)$, $((a/2), -(a/2))$, and $(-(a/2), -(a/2))$, respectively. The subarrays are rotated in ϕ by 0, 90, 180, and 270°, respectively.[1] It is assumed that the array elements have rotationally symmetric radiation patterns. Fig. 2 shows one such block.

Last, the concept of subarray rotation is generalized to allow random rotations. In an array of randomly rotated random subarrays (ARRS-R), the pattern of rotations is not deterministic. The allowed rotation values may be discrete—for example, in Fig. 3 the rotations allowed are 0, 90, 180, and 270°—or they may be a continuum. For this analysis we will require that the subarrays not overlap.

For all three arrays, a and b are subarray dimensions, measured in wavelengths, and P and Q are the numbers of subarrays in the $\phi = 0°$ and $\phi = 90°$ directions, respectively. For the rectangular subarrays of the PARS, a and b denote the sides of the subarrays. Due to its rotations, the ARRS-P is required to have square subarrays whose side length is denoted a. In contrast, the ARRS-R subarrays may take any shape, so a is defined to be the subarrays' largest dimension. N is the number of elements per subarray. The random variables x_n and y_n denote the normalized positions of individual elements in the subarray in a coordinate system local to the subarray. They may vary from −1/2 to 1/2. x_n and y_n have probability distributions $f(x)$ and $g(y)$, respectively. Both distributions shall be required to be even, because it reduces the complexity of calculations and because most arrays in practice have symmetric element placements. In the ARRS-P and ARRS-R, the angle by which a subarray with indices p, q is rotated is denoted ψ_{pq}. The definitions of these variables are illustrated in Fig. 4. For the ARRS-R, we must also define M, the number of allowed values for the rotation angle.

III. Array Factor Analysis

A. Array Factors

For each array geometry, the array factor is the superposition of the patterns of individual isotropic elements. For the PARS, this immediately simplifies into the familiar $sinc$ function of the periodic superarray multiplied by the sum associated with the

[1]When individual circularly polarized elements are rotated in the pattern shown for the ARRS-P, grating lobes arise due to the introduced periodicity. The same rotation pattern was applied again to the four-element subarrays, and it was found that when four subarrays were arranged in a square sixteen-element array, the grating lobes were reduced [11]. This work employs the same rotation pattern in order to demonstrate the effects of non-periodic (a single group of four subarrays) and periodic (more than one group) rotation.

subarrays, as is apparent in this expression for the array factor $G_{\mathrm{PARS}}(\theta,\phi)$

$$G_{\mathrm{PARS}}(\theta,\phi)=\frac{1}{NPQ}\frac{\sin(P\pi a\sin\theta\cos\phi)}{\sin(\pi a\sin\theta\cos\phi)}\times\frac{\sin(Q\pi b\sin\theta\sin\phi)}{\sin(\pi b\sin\theta\sin\phi)}\sum_{n=1}^{N}e^{j2\pi\sin\theta(ax_n\cos\phi+by_n\sin\phi)}. \quad (1)$$

To begin with, we will consider a single four-subarray block of the ARRS-P, and later generalize to arrays of many subarrays. For a single block, the array factor is given by the sum of the subarray factors, with phases adjusted for rotation and position. The array factors of subarrays rotated by 0, 90, 180, and 270° are denoted G_0, G_{90}, G_{180}, and G_{270}, respectively

$$G_0=\frac{1}{N}e^{j\pi a\sin\theta(-\cos\phi+\sin\phi)}\times\sum_n e^{j2\pi a\sin\theta(x_n\cos\phi+y_n\sin\phi)} \quad (2)$$

$$G_{90}=\frac{1}{N}e^{j\pi a\sin\theta(\cos\phi+\sin\phi)}\times\sum_n e^{j2\pi a\sin\theta(-x_n\sin\phi+y_n\cos\phi)} \quad (3)$$

$$G_{180}=\frac{1}{N}e^{j\pi a\sin\theta(\cos\phi-\sin\phi)}\times\sum_n e^{j2\pi a\sin\theta(-x_n\cos\phi-y_n\sin\phi)} \quad (4)$$

$$G_{270}=\frac{1}{N}e^{j\pi a\sin\theta(-\cos\phi-\sin\phi)}\times\sum_n e^{j2\pi a\sin\theta(x_n\sin\phi-y_n\cos\phi)} \quad (5)$$

$$G_{\mathrm{ARRS-P}}(\theta,\phi)=\frac{1}{4}(G_0+G_{90}+G_{180}+G_{270}). \quad (6)$$

The array factor of the ARRS-R is similarly constructed from a sum of subarray factors

$$G_{\mathrm{ARRS-R}}(\theta,\phi)=\frac{1}{NPQ}\sum_{p=1}^{P}\sum_{q=1}^{Q}e^{j2\pi a\sin\theta(p\cos\phi+q\sin\phi)}\times\sum_{n=1}^{N}e^{j2\pi a\sin\theta(x_n\cos(\phi-\psi_{pq})+y_n\sin(\phi-\psi_{pq}))}. \quad (7)$$

B. Expected Value and Variance

Although the element positions are as yet unknown, the likely behavior of the arrays can be predicted using probabilistic methods [4]. In this analysis, we will characterize the approximate shape of the array factor. It is most useful to treat the real and imaginary parts of each array factor separately. The real part of the PARS array factor will be denoted $G_{\mathrm{PARS},R}$, the imaginary part $G_{\mathrm{PARS},I}$, and similar symbols are assigned to the real and imaginary parts of the other arrays' factors.

In the case of the ARRS-P, the particular rotation pattern chosen causes the imaginary part to be identically zero. The real part is then written

$$G_{\mathrm{ARRS-P},R}(\theta,\phi)=\frac{1}{2N}\left(\sum_{n=1}^{N}\cos\left(\pi a\sin\theta(-\cos\phi+\sin\phi+2x_n\cos\phi+2y_n\sin\phi)\right)+\sum_{n=1}^{N}\cos\left(\pi a\sin\theta(\cos\phi+\sin\phi-2x_n\sin\phi+2y_n\cos\phi)\right)\right). \quad (8)$$

Finally, the real and imaginary parts of the ARRS-R array factor are given in (9) and (10) as follows:

$$G_{\mathrm{ARRS-R},R}=\frac{1}{NPQ}\sum_{p=1}^{P}\sum_{q=1}^{Q}\sum_{n=1}^{N}\cos(2\pi a\sin\theta(p\cos\phi+q\sin\phi+x_n\cos(\phi-\psi_{pq})+y_n\sin(\phi-\psi_{pq})) \quad (9)$$

$$G_{\mathrm{ARRS-R},I}=\frac{1}{NPQ}\sum_{p=1}^{P}\sum_{q=1}^{Q}\sum_{n=1}^{N}\sin(2\pi a\sin\theta(p\cos\phi+q\sin\phi+x_n\cos(\phi-\psi_{pq})+y_n\sin(\phi-\psi_{pq})). \quad (10)$$

To compute the expected value and variance of these quantities, we will introduce reduced angle variables u and v, and characteristic functions $\varphi_x(u)$ and $\varphi_y(u)$. The characteristic functions are only coincidentally similar to the functions used in statistical analysis; they actually arise because they are related to the expected array factor of a subarray

$$u=\sin\theta\cos\phi \quad (11)$$

$$v=\sin\theta\sin\phi \quad (12)$$

$$\varphi_x(u)=\int_{-1/2}^{1/2}f(x)e^{j2\pi aux}dx=\int_{-1}^{1}f(x)\cos(2\pi aux)dx \quad (13)$$

$$\varphi_y(v)=\int_{-1/2}^{1/2}g(y)e^{j2\pi bvy}dy=\int_{-1}^{1}g(y)\cos(2\pi bvy)dy. \quad (14)$$

Since $f(x)$ and $g(y)$ are even functions, the integral of the exponential is equivalent to the integral of the cosine.

Because the ARRS-R is more general, it will require slightly modified expressions. Since the cosine and sine factors on x and y occur in pairs, we will define a reduced angle variable sum U_m to replace u and v. Below, ψ_m is the mth allowed rotation angle out of the total M

$$U_m=\sin\theta\,(x\cos(\phi-\psi_m)+y\sin(\phi-\psi_m)) \quad (15)$$

$$\varphi(U_m)=\iint_A\cos(2\pi aU_m)f(x)g(y)dA. \quad (16)$$

The quantity $\varphi(U_m(x,y))$ above is similar to the φ definitions used earlier, but the expression here is more general and does not separate the x and y integrals, since the cosine and sine factors on x and y occur in pairs that depend on the value of ψ for the subarray.

With these definitions in mind, the array factor expected values are as follows. For the PARS

$$E\left(G_{\mathrm{PARS},R}(u,v)\right) = \frac{1}{PQ}\frac{\sin(\pi aPu)}{\sin(\pi au)}\frac{\sin(b\pi Qv)}{\sin(b\pi v)} \times \varphi_x(2\pi au)\varphi_y(2\pi av) \quad (17)$$

$$E\left(G_{\mathrm{PARS},I}(u,v)\right) = 0. \quad (18)$$

For the ARRS-P

$$E\left(G_{\mathrm{ARRS-P},R}(u,v)\right) = \frac{1}{2}\left(\cos\left(\pi a(u-v)\right)\varphi_x(2\pi au) \times\varphi_y(2\pi av) + \cos\left(\pi a(u+v)\right)\varphi_x(2\pi av)\varphi_y(2\pi au)\right). \quad (19)$$

And for the ARRS-R

$$E(G_{\mathrm{ARRS-R},R}) = \frac{1}{PQM}\iint_A \sum_{(p,q)=(1,1)}^{(P,Q)}\sum_{m=1}^{M}\cos\left(2\pi a\left(pu+qv+U_m(x,y)\right)\right) \times f(x)g(y)dA \quad (20)$$

$$E(G_{\mathrm{ARRS-R},I}) = \frac{1}{PQM}\iint_A \sum_{(p,q)=(1,1)}^{(P,Q)}\sum_{m=1}^{M}\sin\left(2\pi a\left(pu+qv+U_m(x,y)\right)\right) \times f(x)g(y)dA. \quad (21)$$

In (20) and (21), A is the aperture of a subarray and dA is a differential area element. If the shape of the subarrays is symmetric in x and y, then dA is an even function of both, and these expressions simplify to

$$E(G_{\mathrm{ARRS-R},R}) = \frac{1}{PQM}\sum_{(p,q)=(1,1)}^{(P,Q)}\sum_{m=1}^{M}\cos\left(2\pi a(pu+qv)\right) \times \varphi(2\pi aU_m) \quad (22)$$

$$E(G_{\mathrm{ARRS-R},I}) = \frac{1}{PQM}\sum_{(p,q)=(1,1)}^{(P,Q)}\sum_{m=1}^{M}\sin\left(2\pi a(pu+qv)\right) \times \varphi(2\pi aU_m). \quad (23)$$

In the region of the main beam, the array factor is nearly deterministic. It is very likely to have the shape of the array factor's expected value [12]. In the sidelobe region this is not the case, so it remains for us to characterize the sidelobe level (SLL) in order to arrive at an accurate idea of the array's behavior. It is helpful that, by the Riemann-Lebesque theorem, φ terms will go to zero in the sidelobe region. As a result, in that region all of the expected values are approximately zero.

By the same reasoning, approximations can also be made to the variances of the real and imaginary parts of each array factor in the sidelobe region. The approximate variances are given below. For the PARS

$$\sigma^2_{\mathrm{PARS},R} = \sigma^2_{\mathrm{PARS},I} \approx \left(\frac{1}{PQ}\frac{\sin(a\pi Pu)}{\sin(a\pi u)}\frac{\sin(b\pi Qv)}{\sin(b\pi v)}\right)^2 \times \frac{1}{2N}. \quad (24)$$

Since the imaginary part of the ARRS-P array factor is identically zero, the variance of the imaginary part must be zero. The variance of the real part is

$$\sigma^2 \approx \frac{1}{4N}. \quad (25)$$

Lastly, the variances for the real and imaginary parts of the ARRS-R array factor are

$$\sigma^2_{\mathrm{ARRS-R},R} = \sigma^2_{\mathrm{ARRS-R},I} \approx \frac{1}{2NPQ} + \frac{1}{2NMP^2Q^2} \times \left(\left(\frac{\sin\left(a\pi u(P+1)\right)}{\sin(a\pi u)} \times\frac{\sin\left(a\pi v(Q+1)\right)}{\sin(a\pi v)}\right)^2 - PQ\right). \quad (26)$$

In the special case where M is very large (corresponding to a continuum of allowed rotation angles), the variances for the ARRS-R are approximately equal and given by the simpler expression

$$\sigma^2_{\mathrm{ARRS-R},R} \approx \sigma^2_{\mathrm{ARRS-R},I} \approx \frac{1}{2NPQ}. \quad (27)$$

C. Probability Distributions

By the central limit theorem, if N (and, in the case of the ARRS-R, the product PQ) is large, then each of the real and imaginary parts of all of these array factors is an approximately normally distributed random quantity. In that case, the magnitudes of the PARS and ARRS-R array factors at any particular observation angle have chi-squared distributions with two degrees of freedom, and the sidelobes of the ARRS-P array factor have a normal distribution. This can be used to arrive at a probability distribution for the height of a particular sidelobe.

For the PARS, the probability that a sidelobe is less than some fraction r of the main beam is given by

$$\Pr\left\{\left|G_{\mathrm{PARS}}(u_1,v_1)\right| < r\right\} = 1 - e^{-r^2/2\sigma^2}. \quad (28)$$

Since $\sigma^2_R = \sigma^2_I$, we can use a single quantity σ^2.

In the case of the ARRS-P, the probability distribution of the sidelobe magnitude is

$$\Pr\left\{\left|G_{\mathrm{ARRS-P}}(u_1,v_1)\right| < r\right\} \approx \mathrm{Erf}(r\sqrt{2N}). \quad (29)$$

When considering the ARRS-R, we may either look at the case where M is large and we can use the approximate variance from (27), or the case where M is not large and we must use the variance from (26). In terms of utility, we are more interested in the case where M is large because in that case the whole variance depends on $1/PQ$. If M is small only one of the terms depends on $1/PQ$—the $sinc^2$ in the second term sometimes cancels out the P^2Q^2 in the denominator, depending on the angle. Because of this, the case of large M is the more interesting case and from now on it will be the only type of ARRS-R considered. The probability distribution of the magnitude of a sidelobe for this case is

$$\Pr\{|G(u_1,v_1)|<r\}=1-e^{-NPQr^2}. \tag{30}$$

From these probability distributions, the expected value of the SLL, which predicts the average SLL, can be computed for each type of array. Since the PARS SLL has a chi-squared distribution, it is known that the average SLL for a given location must be $2\sigma_{\mathrm{PARS}}$. However, since the variance of the PARS SLL is angle-dependent, we must also average over the solid angle occupied by the sidelobes. Assuming the main beam is narrow, we can express the PARS average SLL as follows:

$$r_{\mathrm{avg}}=\frac{1}{4\pi}\int\int(2\sigma_{\mathrm{PARS}})\sin\theta d\theta d\phi \tag{31}$$

The sidelobe value of the ARRS-P has a normal distribution, and we must take its absolute value in order to calculate the average SLL in a useful way

$$r_{\mathrm{avg}}^2=\int_{-\infty}^{\infty}2\sqrt{\frac{2N}{\pi}}r'^2e^{-2Nr'^2}dr'=\left(\frac{1}{2\sqrt{N}}\right)^2. \tag{32}$$

The average SLL of the ARRS-R is obtained directly from the properties of a chi-squared distribution with two degrees of freedom:

$$r_{\mathrm{avg}}=\frac{2}{\sigma_{\mathrm{ARRS-R}}}=\sqrt{\frac{2}{NPQ}}. \tag{33}$$

The probability distribution of the peak SLL can be approximately characterized by a joint probability distribution of many individual sidelobes [12]. Because of the angle-dependent variance of the PARS, it is clear that the highest sidelobes are likely to be at the locations of grating lobes in the superarray pattern. At those locations, the variance is $1/2N$ and the probability distribution of the PARS peak sidelobe level is

$$\Pr\{|G_{\mathrm{ARRS-R}}(u,v)|<r\forall(u,v)\text{ outside main beam}\}=\left(1-e^{-Nr^2}\right)^{4ab}. \tag{34}$$

For the ARRS-P and ARRS-R, the variance is approximately independent of observation angle, so we must observe enough locations that the joint probability will be representative. For Lo's analysis of a purely random array the number of locations observed was 16 × (array area in square wavelengths) [4]. Applying this to the ARRS-P, we obtain

$$\Pr\{|G_{\mathrm{ARRS-P}}(u,v)|<r\forall(u,v)\text{ outside main beam}\}\approx\left(\mathrm{Erf}(r\sqrt{2N})\right)^{64a^2}. \tag{35}$$

If there is more than one block of four subarrays in an ARRS-P, the blocks themselves may be treated as subarrays in a PARS. In that case, the probability distribution becomes

$$\Pr\{|G_{\mathrm{ARRS-P}}(u,v)|<r\forall(u,v)\text{ outside main beam}\}\approx\left(\mathrm{Erf}(r\sqrt{2N})\right)^{16a^2}. \tag{36}$$

Applying the same method to the ARRS-R

$$\Pr\{|G_{\mathrm{ARRS-R}}(u,v)|<r,\forall(u,v)\text{ outside main beam}\}=\left(1-e^{-NPQr^2}\right)^{16PQa^2}. \tag{37}$$

IV. Array Behavior

The goal of this work is to arrive at a new type of array that duplicates the wideband capabilities of purely random arrays while improving manufacturability by simplifying the geometry. This section will compare how well the three new types of arrays that have been presented meet that objective. Section III's probabilistic analyses will be employed to compare characteristics such as the number of elements needed to meet a particular peak SLL requirement, the relative peak sidelobe levels achievable by arrays with the same number of elements and aperture size, the extent to which division into subarrays is practical for simplifying the geometry, and the directivities achievable with each type of array.

A. Probabilistic Comparison of Array Properties

Figs. 5 and 6 show the peak SLL probability distribution for all three arrays discussed here versus r for arrays of four and sixteen subarrays, respectively. As is evident in these figures, the peak sidelobe levels of all three arrays exhibit threshold behavior in r. There is a threshold where the probability of a successful array increases sharply and beyond which it is nearly 1, increasing very slowly. Similar behavior can be observed in the plots of peak SLL versus N (Figs. 7 and 8).

This is the foundation of the wide bandwidth capability of random arrays; if N and r are chosen to be above threshold over the entire frequency range, an array with those parameters is almost certain to have acceptable sidelobe levels throughout that range. Fig. 9 shows the variation of the peak SLL probability distribution with subarray dimension a (in this example the subarrays are all square), which is proportional to frequency. In Fig. 9, N is sufficient for the ARRS-R probability to remain very close to 1 over the entire frequency range while the ARRS-P and PARS probabilities fall off more quickly.

Comparing the peak SLL probability distribution's dependence on r and N provides information about the relative sidelobe levels achievable with each type of array. For an array of

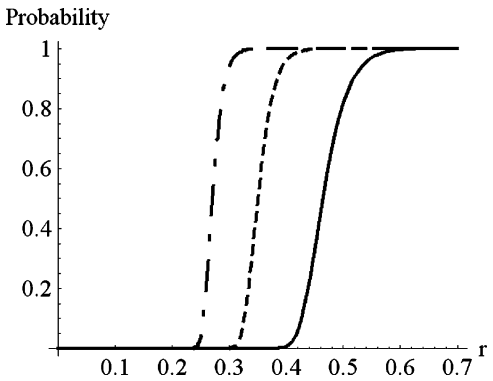

Fig. 5. Peak SLL probability distribution versus r for PARS (solid line), ARRS-P (dashed line), and ARRS-R (dot-dashed line). Each array has four $20\lambda \times 20\lambda$ subarrays of 36 elements.

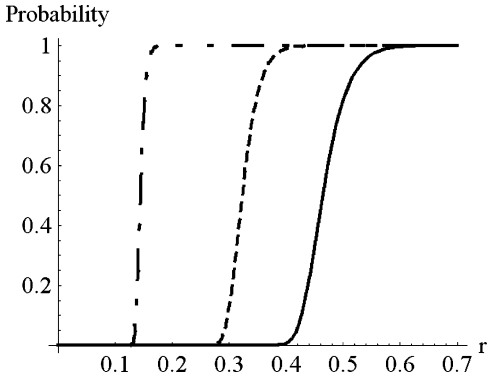

Fig. 6. Peak SLL probability distribution versus r for PARS (solid line), ARRS-P (dashed line), and ARRS-R (dot-dashed line). Each array has sixteen $20\lambda \times 20\lambda$ subarrays of 36 elements.

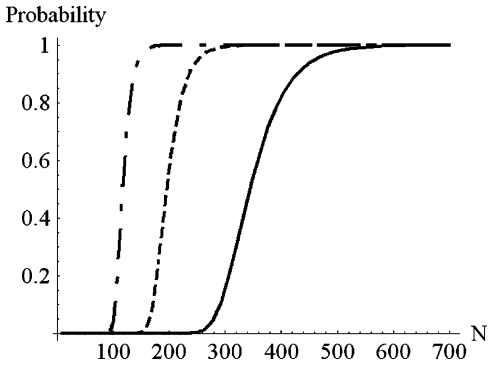

Fig. 7. Peak SLL probability distribution versus N for PARS (solid line), ARRS-P (dashed line), and ARRS-R (dot-dashed line). Each array has four $20\lambda \times 20\lambda$ subarrays, and r is 0.15.

four subarrays, the probability distributions for the ARRS-P and ARRS-R are almost identical, which is expected because they work on the same principle. In the case of four subarrays, the ARRS-P effectively counts as a single, diagonally symmetric random array, so its probability distribution is that of a symmetric array with $4N$ elements. As the number of subarrays grows, however, it will lose this advantage. The probability distribution for the PARS has a considerably higher threshold because the variance of its probability distribution depends only on the number of elements in the subarray. Fig. 6 demonstrates

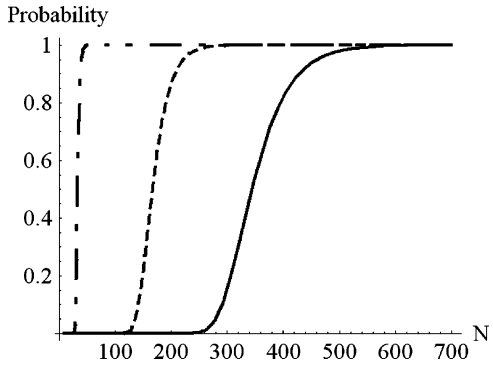

Fig. 8. Peak SLL probability distribution versus N for PARS (solid line), ARRS-P (dashed line), and ARRS-R (dot-dashed line). Each array has sixteen $20\lambda \times 20\lambda$ subarrays, and r is 0.15.

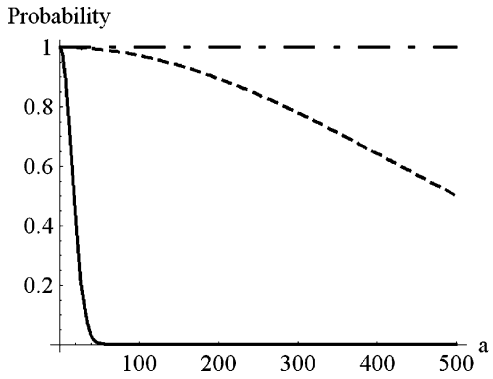

Fig. 9. Peak SLL probability distribution versus a for PARS (solid line), ARRS-P (dashed line), and ARRS-R (dot-dashed line). Each array has four subarrays, $N = 750$ and $r = 0.1$.

what happens to the ARRS-P when there are more than four subarrays. Recall (36), the probability distribution for an ARRS-P with more than four subarrays. Like the PARS, the ARRS-P gains no further advantage in SLL as the number of subarrays increases. The ARRS-R, on the other hand, gets a substantial improvement in the threshold of its probability distribution due to the increase in number of subarrays.

These figures show probability distributions for all three array types for four-subarray and sixteen-subarray cases. Clearly, as the number of subarrays increases, the sidelobe levels of the ARRS-P and PARS essentially stop improving, while that of the ARRS-R can achieve lower sidelobe levels with fewer elements per subarray as more subarrays are added.

Figs. 10 and 11 plot the number of elements required per subarray for PARS, ARRS-P, and ARRS-R arrays with four and sixteen subarrays, respectively. Again, the abilities of the PARS and ARRS-P to achieve low sidelobe levels are not improved by the addition of more subarrays. The ARRS-R, on the other hand, has the capability to reduce the number of elements that need to be randomly distributed while maintaining the frequency and probabilistic characteristics of a purely random array.

B. Directivity Comparison

Random array design has historically been focused on achieving, with fewer elements than traditional designs, the

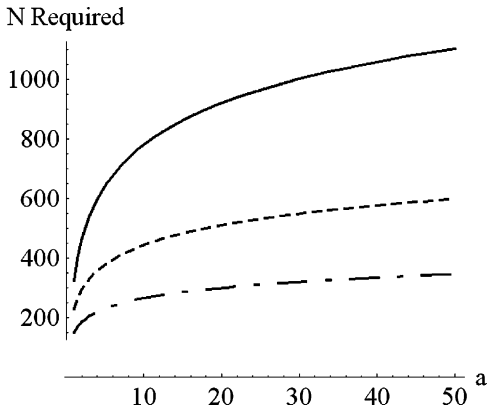

Fig. 10. N required for 85% probability of $r = 0.1$, versus a for an array of four subarrays (PARS: solid line, ARRS-P: dashed line, ARRS-R: dot-dashed line).

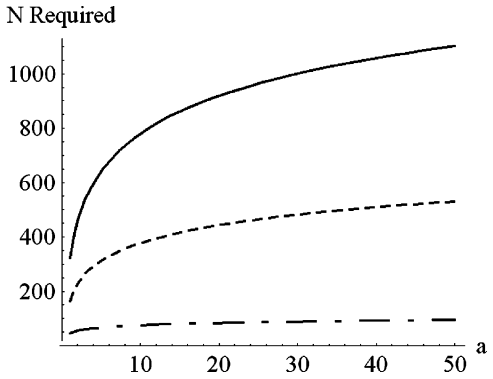

Fig. 11. N required for 85% probability of $r = 0.1$, versus a for an array of sixteen subarrays (PARS: solid line, ARRS-P: dashed line, ARRS-R: dot-dashed line).

narrow beamwidths and low sidelobe levels required for applications like radio astronomy. As a result, many random arrays in the past have had low element density and consequently low directivity. However, the directivity of a random array depends largely on the element density its designer allows, and it is possible to design random arrays with useful directivities for a range of applications. This section will use a simple directivity approximation [14] to illustrate the effect of element density on directivity.

The directivity of an antenna can be defined as

$$D = \frac{4\pi r^2}{\int\int_S p(\theta,\phi) r^2 \sin(\theta) d\theta d\phi} \tag{38}$$

where $p(\theta,\phi)$ is the normalized radiated power [15]. The approximation we will use assumes that, for an antenna with a half-power beamwidth of $2\theta_1$, the normalized power in the main beam is

$$P_{\mathrm{MB}} \approx \frac{4\pi r^2}{3} \sin^2(\theta_1). \tag{39}$$

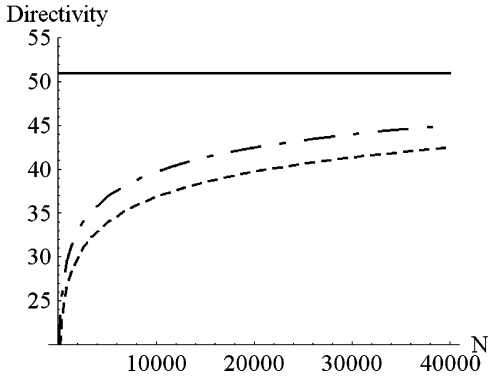

Fig. 12. Directivity (in dB) of ARRS-P (dashed) and ARRS-R (dot-dashed) versus their total number of elements, compared to that of a periodic array with 40,000 elements, held constant. All three arrays are square and have constant aperture $\mathrm{area} = 10,000\lambda^2$; the periodic array has $\lambda/2$ spacing.

Also, if the main beam is narrow, the normalized power radiated in the sidelobes is

$$P_{\mathrm{SL}} \approx 2\pi r^2 \mathrm{SLL}_{av} \tag{40}$$

where SLL_{av} is the average power sidelobe level, which is equal to r_{avg}^2. Combining these three equations, directivity is approximated as

$$D \approx \frac{1}{\frac{1}{3}\sin^2(\theta_1) + \frac{1}{2}\mathrm{SLL}_{av}}. \tag{41}$$

Since the ARRS-P and ARRS-R are the most promising of the arrays presented, we will compare their directivities with that of a uniformly illuminated rectangular aperture with 100% aperture efficiency. From [15], the directivity of such an aperture at broadside is

$$D_{\mathrm{periodic}} = 4\pi A. \tag{42}$$

A periodic array with the same aperture size whose element spacing is a half wavelength has the same directivity as this aperture [15].

Using the directivity approximation from (41), an approximate beamwidth [15], and the average sidelobe levels from (32) and (33), Fig. 12 compares the directivity of the ARRS-P and ARRS-R with that of the uniformly illuminated aperture. The ARRS-R in this case has a continuum of allowed rotations. All three have aperture area held constant at 10000 λ^2; everything remains constant about the aperture while the density of elements in the ARRS-P and ARRS-R increases. This comparison is not entirely realistic since it is assumed that the density can arbitrarily increase; in reality elements have a finite size and it becomes more likely that some might overlap as the density increases.

Fig. 12 illustrates that, as one would expect, the directivity of an ARRS-P or ARRS-R goes up as the element density increases. By the time the random arrays have the same element density as the half-wavelength spaced periodic array, their directivities are less by about 8.5 and 6 dB, respectively. When

the element density is much lower, for instance between densities of one element per five square wavelengths and one element per one square wavelength, the directivity is between 21 dB (ARRS-P, 2000 total elements) and 11 dB (ARRS-R, 10,000 total elements) less than that of the periodic array which has four to twenty times more elements. This trade-off in directivity should be considered in conjunction with the greatly increased bandwidth and reduced number of elements of the ARRS-P and ARRS-R.

V. Design Example

It may be illustrative to design a sample array of each type, given some arbitrary specifications. Suppose that an array is desired that operates from 2 to 10 GHz and has a peak SLL of -20 dB. Because the analysis of these arrays depends on the central limit theorem, the number of elements per subarray must be reasonably large. We will require at least 20. Since antennas with wide bandwidths often have larger dimensions, we will restrict the element density to at most one per three square wavelengths to prevent overlapping. A nearest-neighbor constraint could also be imposed, but for a simple example the density requirement should be sufficient. Because smaller subarrays allow greater simplification of feed networks and the overall manufacturing process, an array with many subarrays of a small number of elements is preferred over one with fewer subarrays and more elements per subarray.

In this section, plots of each array factor will be presented for only the highest frequency in the selected operating band. An array factor can be considered an arbitrary function of au and av, where a, the subarray dimension in wavelengths, scales linearly with frequency. For any such function, increasing a will scale the features of the function closer together in u and v, but the features themselves will be otherwise unchanged. By this reasoning, a plot of an array factor at the highest point in the operating band indicates the array's behavior over the entire band.

If we require that the probability of success be 85%, to reduce the chances of our having to test more than one array, this set of requirements results in a PARS with 1309 elements per subarray. Assuming the subarrays are square, they would measure 62.67 wavelengths on a side at 2 GHz, or about 9.40 m. Fig. 13 shows the radiation pattern of this array at 10 GHz.

In the case of an ARRS-P, the elements decrease the SLL most efficiently if there are four subarrays. Predetermining the number of subarrays selects whether the array is described by (35) or by (36). Having determined that, the same probability requirement we enforced on the PARS now yields an ARRS-P with 664 elements per subarray. These subarrays are required to be square because of the rotation pattern, and they would measure 44.64 wavelengths on a side at 2 GHz, or about 6.70 m. The entire array of four subarrays would also be square, and measure 13.40 m on a side. The total number of elements is 2656. Fig. 14 shows the radiation pattern of this array at 10 GHz.

Lastly, the ARRS-R is considered. Since the ARRS-R peak sidelobe probability distribution can be improved by increasing the total number of elements, rather than the number of elements per subarray, we would like these subarrays to be as small as possible because that furthers our goal of simplifying the geometry. Assuming there are 20 elements per subarray, the resultant array has 72 subarrays and a total of 1440 elements. Because we must allow arbitrary rotation amounts without overlapping, the subarrays are assumed to be circular since that minimizes the surface area. The element density requirement results in subarrays with a diameter of 1.31 m. This distance will also be the spacing a of the subarray grid. If the array is a rectangle of 9 subarrays by 8 subarrays, its dimensions are 10.5 by 11.8 m. Fig. 15 shows the radiation pattern of this array at 10 GHz.

Fig. 16 shows the main beam region of the array factor at 2 GHz of an ARRS-R with properties determined by the sample design. Superarray grating lobes are clearly visible near the main beam. This occurs because the array factor of the subarray is dominated by its expected value in that region, so the subarray patterns are still too similar after rotation to reduce the grating lobes to the same degree that they are reduced in the

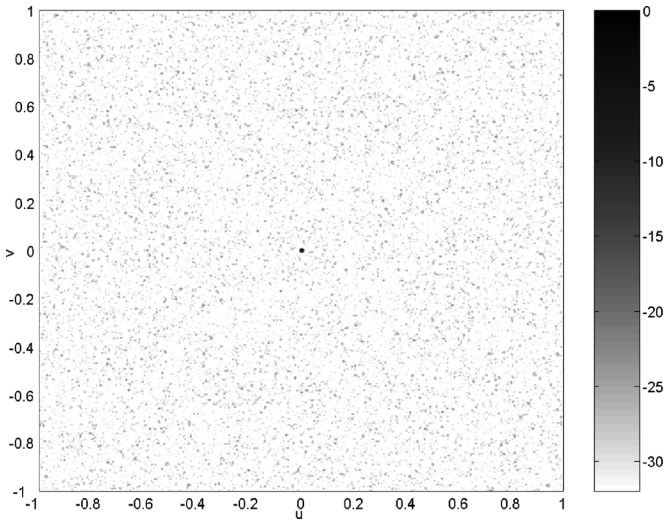

Fig. 13. Array factor at 10 GHz of PARS designed using parameters from sample design: $N = 1309$, $a = b = 634.5\lambda_{10\ \mathrm{GHz}}$, 4 subarrays, normal element distribution.

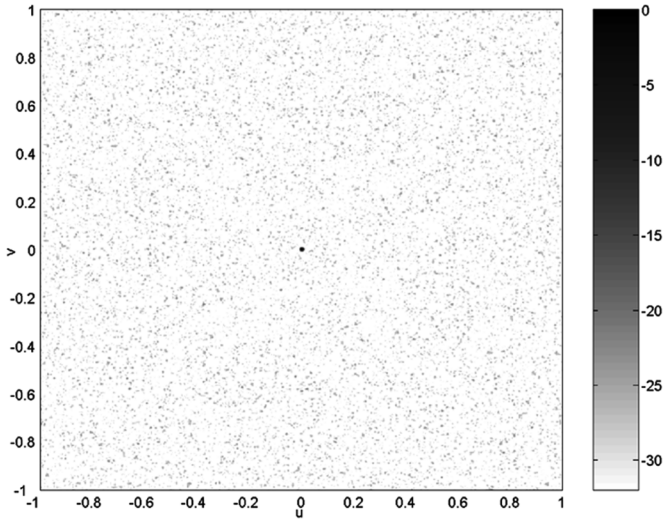

Fig. 14. Array factor at 10 GHz of ARRS-P designed using parameters from the sample design: $N = 664$, $a = b = 223.20\lambda_{10\ \mathrm{GHz}}$, 4 subarrays, normal element distribution.

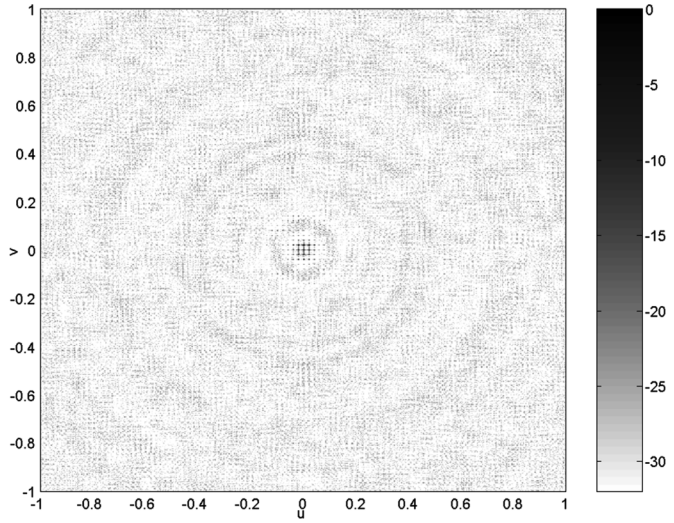

Fig. 15. Array factor at 10 GHz of ARRS-R designed using parameters from sample design: $N = 20$, $a = 43.70\lambda_{10\,\mathrm{GHz}}$, 72 subarrays, normal element distribution.

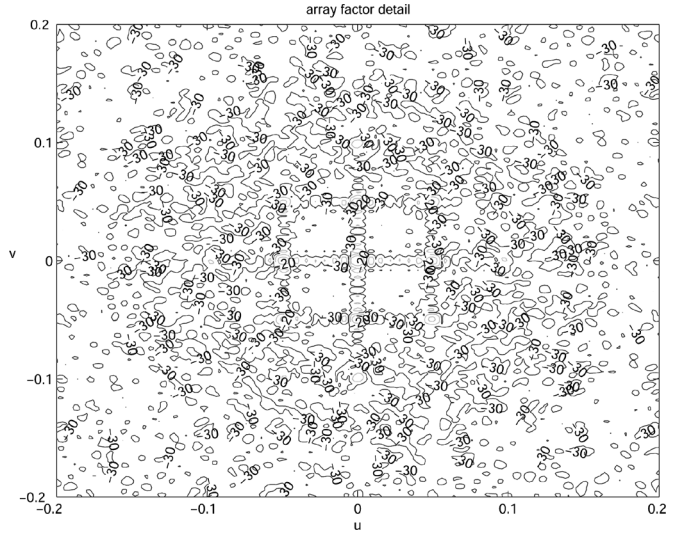

Fig. 16. Main beam region of array factor at 2 GHz of ARRS-R designed using parameters from sample design: $N = 20$, $a = 8.74\lambda_{2\,\mathrm{GHz}}$, 72 subarrays, normal element distribution.

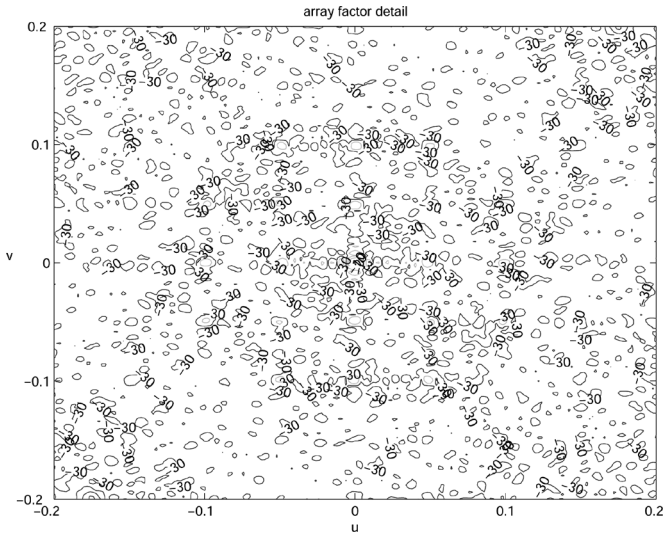

Fig. 17. Main beam region of array factor at 2 GHz of ARRS-R designed using parameters from sample design: $N = 20$, $a = 8.74\lambda_{2\,\mathrm{GHz}}$, 72 subarrays, uniform element distribution.

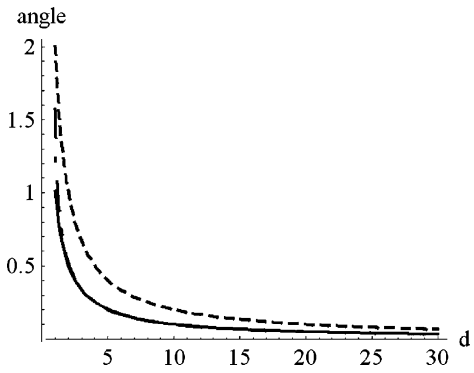

Fig. 18. Beamwidth between first nulls (dotted line) and half-power beamwidth (solid line) for subarray with dimension d, compared to first grating lobe location of superarray with grid spacing d (dot-dashed line). Angles in radians.

far sidelobe region. It is important to note that, since the shape of the subarray main beam depends strongly on the element distribution, a tapered element distribution in the subarray is likely to result in more prominent first grating lobes because the subarray main beam will be wider. Indeed, if one compares Fig. 17, in which the subarrays have a uniform element distribution, with Fig. 16, where the element distribution is normal, it is apparent that fewer grating lobes are visible above the random sidelobe variation.

It is probably not possible to entirely eliminate these grating lobes in this type of array, since the first grating lobe location for the superarray pattern is very near the predicted half-power beamwidth of a subarray with uniform element distribution (Fig. 18). However, the grating lobes have significantly less than half the power of the main beam, which implies that the subarray rotation is having some effect on the SLL.

VI. Conclusion

This investigation has yielded two useful new arrays: the ARRS-P arrangement can be used for an array with a small number of subarrays, and the ARRS-R generalizes the rotation approach to an arbitrary number of subarrays. The arrays were intended to update the random array concept for the present-day demands of fabrication while preserving its bandwidth capability. The ARRS-R has accomplished that goal quite well, transforming the purely random array into many small identical subarrays while almost duplicating the purely random array's performance.

Since none of these arrays has been constructed, one portion of planned future work is an experiment much like the holey-plate experiment performed by Lo [16]. To reduce the size of the array so that measurement is practically feasible, the array will be scaled down and the experiment performed in the optical regime [17], [18]. Since the utility of the ARRS-R is improved if the subarrays are allowed to have fewer elements, one future investigation of this topic could focus on the effect of small N on the accuracy of this analysis. Also, as was mentioned in the

introduction, the rotation method can be applied to other, possibly optimized types of aperiodic arrays.

REFERENCES

[1] D. D. King, R. F. Packard, and R. K. Thomas, "Unequally spaced, broad-band antenna arrays," *IEEE Trans. Antennas Propag.*, vol. 8, pp. 380–384, Jul. 1960.

[2] M. G. Andreasen, "Linear arrays with variable interelement spacings," *IEEE Trans. Antennas Propag.*, vol. 10, pp. 137–143, Mar. 1962.

[3] G. W. Swenson and Y. T. Lo, "The University of Illinois radio telescope," *IEEE Trans. Antennas Propag.*, vol. 9, pp. 9–16, Jan. 1961.

[4] Y. T. Lo, "A mathematical theory of antenna arrays with randomly spaced elements," *IEEE Trans. Antennas Propag.*, vol. 12, pp. 257–268, May 1964.

[5] ——, "A probabilistic approach to the problem of large antenna arrays," *Radio Science*, vol. 68D, pp. 1011–1019, Sep. 1964.

[6] B. D. Steinberg, "Comparison between the peak sidelobe of the random array and algorithmically designed aperiodic arrays," *IEEE Trans. Antennas Propag.*, vol. 21, pp. 366–370, May 1973.

[7] W. J. Hendricks, "The totally random versus the bin approach for random arrays," *IEEE Trans. Antennas Propag.*, vol. 39, pp. 1757–1762, Dec. 1991.

[8] R. L. Fante, G. A. Robertshaw, and S. Zamoscianyk, "Observation and explanation of an unusual feature of random arrays with a nearest-neighbor constraint," *IEEE Trans. Antennas Propag.*, vol. 39, pp. 1757–1762, Jul. 1991.

[9] M. G. Bray, D. H. Werner, D. W. Boeringer, and D. W. Machuga, "Optimization of thinned aperiodic linear phased arrays using genetic algorithms to reduce grating lobes during scanning," *IEEE Trans. Antennas Propag.*, vol. 50, pp. 1732–1742, Dec. 2002.

[10] J. Robinson and Y. Rahmat-Samii, "Particle swarm optimization in electromagnetics," *IEEE Trans. Antennas Propag.*, vol. 52, pp. 397–407, Feb. 2004.

[11] P. S. Hall and M. S. Smith, "Sequentially rotated arrays with reduced sidelobe levels," *Proc. Inst. Elect. Eng. Microwave Antennas Propagation*, vol. 141, pp. 321–325, Aug. 1994.

[12] Y. T. Lo, *On the Theory of Randomly Spaced Antenna Arrays* Antenna Lab., Dept. of Elec. Engrg., Univ. of Illinois, Urbana, Tech. Rep. GI4894, 1962, Sponsored by Nat. Science Foundation.

[13] ——, "Sidelobe level in nonuniformly spaced antenna arrays," *IEEE Trans. Antennas Propag.*, vol. 11, pp. 511–512, Jul. 1963.

[14] R. Kinsey, *Private Communication.* 2004.

[15] J. D. Kraus and R. J. Marhefka, *Antennas For All Applications*, 3rd ed. New York: McGraw-Hill, 2002.

[16] Y. T. Lo and R. J. Simcoe, "An experiment on antenna arrays with randomly spaced elements," *IEEE Trans. Antennas Propag.*, vol. 15, pp. 231–235, Mar. 1967.

[17] M. I. Skolnik, "A method of modeling array antennas," *IEEE Trans. Antennas Propag.*, vol. 12, pp. 97–98, Jan. 1963.

[18] W. H. Huntley, Jr., "A new approach to antenna scaling," *IEEE Trans. Antennas Propag.*, vol. 11, pp. 591–592, Sep. 1963.

Kiersten C. Kerby (S'06) received the B.S. and M.S. degrees in electrical engineering from the University of Illinois at Urbana Champaign (UIUC), in 2003 and 2005, respectively. She is currently working toward the Ph.D. degree in electrical engineering at UIUC.

Her research interests include antennas and applications at microwave, millimeter-wave, and submillimeter-wave frequencies.

Ms. Kerby is a recipient of the Bell Labs Graduate Research Fellowship for 2006–2007.

Jennifer T. Bernhard (S'89–M'95–SM'01) was born on May 1, 1966, in New Hartford, NY. She received the B.S.E.E. degree from Cornell University, Ithaca, NY, in 1988, and the M.S. and Ph.D. degrees in electrical engineering from Duke University, Durham, NC, in 1990 and 1994, respectively, with support from a National Science Foundation Graduate Fellowship.

During the 1994–95 academic year she held the position of Postdoctoral research associate with the Departments of Radiation Oncology and Electrical Engineering at Duke University, where she developed RF and microwave circuitry for simultaneous hyperthermia (treatment of cancer with microwaves) and MRI (magnetic resonance imaging) thermometry. At Duke, she was also an organizing member of the Women in Science and Engineering (WISE) Project, a graduate student-run organization designed to improve the climate for graduate women in engineering and the sciences. From 1995 to 1999, she was an Assistant Professor in the Department of Electrical and Computer Engineering at the University of New Hampshire, where she held the Class of 1944 Professorship. In 1999 and 2000, she was a NASA-ASEE Summer Faculty Fellow at NASA Glenn Research Center in Cleveland, OH. From 1999 to 2003, she was an Assistant Professor in the Department of Electrical and Computer Engineering at University of Illinois at Urbana-Champaign (UIUC). Since 2003, she has held the position of Associate Professor at UIUC. Her industrial experience includes work as a research engineer with Avnet Development Labs and, more recently, as a private consultant for members of the wireless communication and sensors community. Her research interests include reconfigurable and wideband microwave antennas and circuits, wireless sensors and sensor networks, high speed wireless data communication, electromagnetic compatibility, and electromagnetics for industrial, agricultural, and medical applications.

Prof. Bernhard is a member of URSI Commissions B and D, Tau Beta Pi, Eta Kappa Nu, Sigma Xi, and ASEE. She received the NSF CAREER Award in 2000. She is also a UIUC College of Engineering Willett Faculty Scholar and a Research Associate Professor in UIUC's Micro and Nanotechnology Laboratory and the Coordinated Science Laboratory. She and her students received the 2004 H. A. Wheeler Applications Prize Paper Award from the IEEE Antenna and Propagation Society for their paper published in the March 2003 issue of the IEEE TRANSACTIONS ON ANTENNAS AND PROPAGATION. She is serving as an elected member of the IEEE Antennas and Propagation Society's Administrative Committee from 2004–2006. She has served as an Associate Editor for IEEE TRANSACTIONS ON ANTENNAS AND PROPAGATION since 2001 and served as an Associate Editor for IEEE ANTENNAS AND WIRELESS PROPAGATION LETTERS from 2001–2005. She is also a member of the editorial board of *Smart Structures and Systems*.